JOURNAL OF SPACECRAFT AND ROCKETS
Vol. 37, No. 1, January–February 2000

Design Evaluation of a Large Deployable Mesh Reflector

Hiroaki Tsunoda,* Ken-ichi Hariu,† and Yoichi Kawakami‡
Advanced Space Communications Research Laboratory, Tokyo 101-0032, Japan
and
Toshio Sugimoto§ and Kazuo Miyoshi¶
Mitsubishi Electric Corporation, Kanagawa 247-8520, Japan

The deployment force over the deployment resistance force must be considered in the deployment force design of deployable mesh reflectors. Deployment tests are usually conducted on the ground using gravitational force compensation to evaluate the deployment force design. The design evaluations resulting from deployment tests using a test object with a diameter of 7 m are described. Twenty-four magnetically suspended sliders were also used to suspend the test object to reduce the frictional loss of horizontal motion and to compensate for gravitational force. The deployment force is designed as three times the mesh reaction force and is generated by helical coil springs. The complete deployment performance is confirmed by three deployment tests. An increase in the deployment resistance force is verified through asynchronous deployment of the deployable structures and the gravitational force compensation error of the mesh surface. Surface accuracy tests and static load tests under the same configurations as the deployment test were conducted to confirm that a large deployable mesh reflector with a 1.0-mm-rms error surface and 0.13-Hz structural rigidity can be achieved.

Nomenclature

F = deployment force, N
f_1 = first natural frequency, Hz
I = inertial moment, kgm^2
k = equivalent rotation spring stiffness, kgm^2/s^2
R_f = resistance force caused by friction, N
R_g = resistance force caused by gravitational force, N
R_m = mesh reaction force, N
R_{mg} = mesh reaction force with gravity effect, N
T = tension of deploying velocity control cable (deployment force margin), N
θ = deployment angle (bending angle of the top bending bar; 0 stowed and 180 deployed), deg

Introduction

LARGE onboard antennas are required in the field of mobile satellite communications using a geostationary orbit and microwave power transmissions, as well as for space observations.[1–3] These antennas require aperture diameters of over 10 m. Various structural concepts have been proposed for large deployable reflectors. These concepts can be classified into two categories: inflatable-type reflectors[4,5] and metal-mesh-type reflectors.[6–9] The inflatable-type reflector shape is maintained by a thin film surface, which is expanded by gases. The shape of a metal-mesh-type reflector is maintained by the mesh surface, which is supported by cable networks and rigid deployable structures. Different aspects of metal mesh surfaces have been studied to construct highly accurate reflectors. Antennas for communication satellites also require an offset-type reflector to avoid blocking by feeders.

The mesh surface generates the maximum reaction force just before deployment completion. Frictional force in the hinges and the gravitational force acting on the structure act as resistance forces that disturb the deployment. A deployable structure must exert sufficient deployment force against these resistance forces. However, increasing the deployment force necessitates a heavier reflector with huge deployment mechanisms. Therefore, the deployment force design must offer the optimum deployment force. Deployment tests under quasi-static conditions are necessary to compare the results of the deployment analyses. Springs are suitable for generating the deployment force. Motors and cables are also suitable for controlling the deploying velocity when deploying a large mesh reflector.[9–11] Large deployable reflectors also require a 1.0-mm-rms surface accuracy and over 0.1-Hz structural rigidity. Evaluation of these characteristics under microgravity conditions is an important element in developing large deployable antennas.

There are several methods to obtain microgravity conditions, such as using the parabolic flight of an airplane, a space environment, free fall in a vacuum tube, or the buoyant force in water. They each have both advantages and disadvantages in terms of cost, facilitation, testing time, dimensions of the test objects, and damage to the test objects. For example, a microgravity experiment using the parabolic flight of an airplane is often conducted in deployment tests for deployable space structures. This method offers a good microgravity environment, but the scale of the test object is restricted to 20 m (length) × 5 m (width) × 2.5 m (height), and the continuous testing time is restricted to 30 s (in the case of the Airbus A300). Therefore, this test method is mainly used to confirm the deployment functions of a basic test object.

Various test methods on the ground have been adopted to test large space deployable structures. For example, counterweights were used on the tension truss antenna of the MUSES-B satellite to compensate for the gravity effect of the six extendible masts; balloons were also used for the reflector surface.[7] This method is suitable for a deployable structure with a simple and straightforward deployment locus; however, it is difficult to apply to an offset-type reflector because of the complex deployment locus. The Hexa-Link Truss structure, an offset reflector, was suspended by cables from a high ceiling during the deployment test under gravity compensation.[12] This test method can follow a three-dimensional motion, but the resisting forces increase as deployment progresses because the cable slant increases. An appropriate test method is required to obtain test data repeatedly

Received 5 November 1998; revision received 28 April 1999; accepted for publication 19 May 1999.

*Head, On-Board Antenna Technology Section, Chiyoda-ku; currently Senior Research Engineer, Wireless Systems Innovation Laboratory, NTT Network Innovation Laboratories, 1-1, Hikarinooka, Yokosuka-shi, Kanagawa 239-0847, Japan. Senior Member AIAA.

†Senior Research Engineer, On-Board Antenna Technology Section, Chiyoda-ku; currently Engineer, Space Systems Department, Kamakura Works, Mitsubishi Electric Corporation, 325, Kami-Machiya, Kamakura-shi, Kanagawa 247-8520, Japan.

‡Manager, On-Board Technology Department, 7F, Hayakawa-Tonakai Building, 2-12-5, Iwamoto-cho, Chiyoda-ku.

§Senior Engineer, Space Systems Department, Mechanical Engineering Section, Kamakura Works, 325, Kami-Machiya, Kamakura-shi.

¶General Manager, Space Systems Department, Kamakura Works, 325, Kami-Machiya, Kamakura-shi; currently Manager, Electromagnetic Waves Equipment Department, Shoryo Electronic Corporation, 214, Kami-Machiya, Kamakura-shi, Kanagawa 247-0065, Japan.

in the research phase. Verification of the deployment characteristics of a large mesh reflector under high-precision gravity-compensating conditions has not yet been reported.

We have presented a deployment test method for a large deployable mesh reflector using a newly developed deployment test system, as described in Ref. 11. The paper clarified the high-precision deployment test methods by comparing the suspension techniques using magnetically suspended sliders. We will apply that test method to the deployment test of a test object with a diameter of 7 m and evaluate the deployment characteristics. This process is essential to establish the design method for a full-scale reflector (aperture diameter of 10 m) with the same design concept. This paper aims to estimate the deployment characteristics, surface accuracy, and structural rigidity of a 10-m-class deployable reflector that is difficult to test on the ground. This will be achieved through tests and calculations using a 7-m-diam test object, representing the center part of a full-scale reflector. Practical knowledge regarding the characteristics of a full-scale reflector can obtained from the test object. The mechanical characteristics of a full-scale reflector are also estimated in this study.

We will first describe the structural concept of the 7-m-diam test object. Next, we characterize the deployment test methods for the test object, applying the results obtained in previous research[11] that verified that the most effective hanging method uses magnetically suspended sliders. The deployment characteristics are then clarified by an evaluation of the deployment force margin and the deployment resistance force. Finally, the mechanical characteristics, including the surface accuracy and structural rigidity, are determined by surface measurements and static load tests.

Deployment Force Design

Deployable Structure[11]

The test object described in this paper and shown in Fig. 1b has a diameter of 7 m, representing the center part of a full-scale 10-m-diam reflector, shown in Fig. 1a. This test object is constructed from seven hexagonal pyramid-shaped structures. The structure parts are depicted in Fig. 2. The deployment force is provided by helical coil springs equipped on both sides of the top bending bars. The deploying velocity is controlled using deploying velocity control mechanisms. The locations of the deploying velocity control mechanisms are shown in Fig. 1. The deploying velocity control mechanisms in the test object are located in the same positions as on the full-scale reflector.

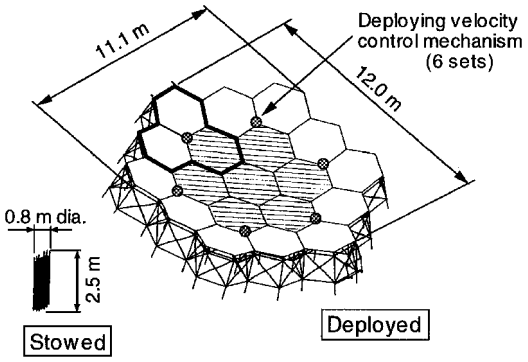

a) Full-scale, 10-m-diam reflector

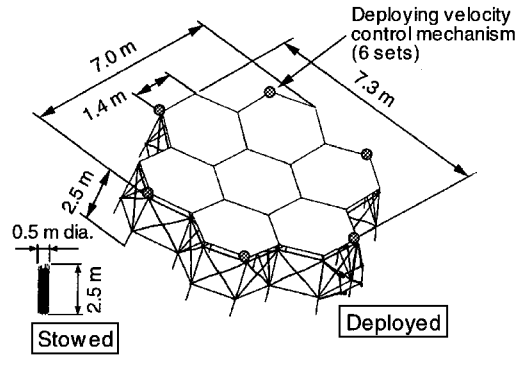

b) 7-m-diam test object

Fig. 1 Configurations of a full-scale reflector and test object.[11]

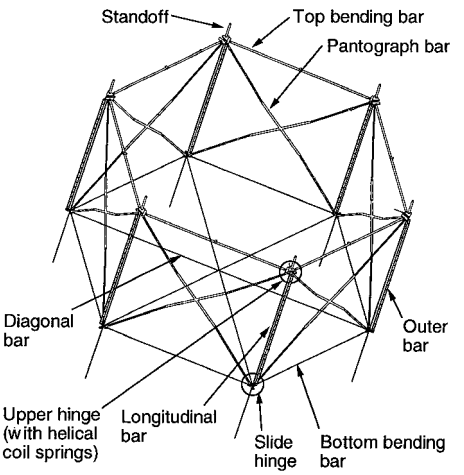

Fig. 2 Structure parts of the deployable structure.[11]

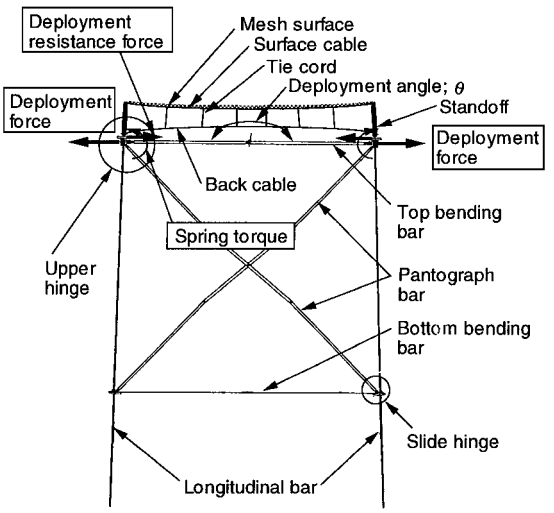

Fig. 3 Side view of the deployable structure.

Mesh Surface

The side view of the deployable structure is shown in Fig. 3. The mesh surface is supported by a cable network to maintain its parabolic shape. The surface and back cables are made of Kevlar 149 (the core; Kevlar is a trademark of Dupont) and Cornex (the envelope; Cornex is a trademark of Teijin). The tie cords (with a diameter of 0.2 mm) are made of Kevlar 49 (the core) and Cornex (the envelope). The test object was constructed with a substitute mesh that simulates the surface density and mesh stiffness, instead of a metal mesh made of gold-plated molybdenum wire. The substitute mesh is 80% nylon and 20% polyurethane with a surface density of 78.9 g/m^2 (the metal mesh is 51.9 g/m^2). A slight surface error occurs under gravity conditions because of the differences in surface densities. The analytical model for calculating the surface shape uses the properties of the substitute mesh.

Deployment Force

The mesh reaction force increases in the last stage of deployment, and the frictional force of the hinges is always present during deployment. The most important factor in deployment force design is generating sufficient deployment force to the top bending bars over the deployment resistance forces. A flowchart of the deployment force design is shown in Fig. 4. First, R_m at the standoffs is calculated from the surface shape analysis. This value is treated as the interface condition between the mesh surface and the deployable structure. Next, the deployment force of the deployable structure is calculated based on the interface value of the mesh reaction force.

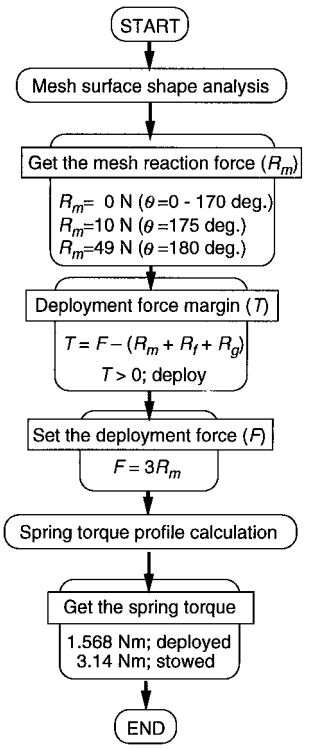

Fig. 4 Flowchart of the deployment force design.

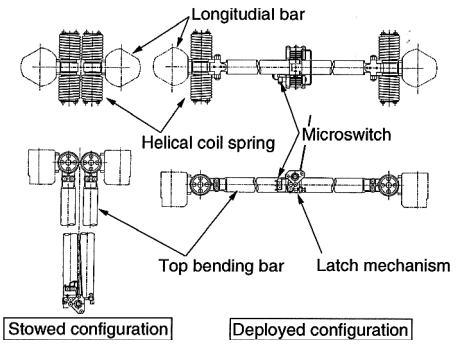

Fig. 5 Installation of helical coil springs on the top bending bar.

The deployment resistance forces in addition to the mesh reaction force are the frictional force at the hinges R_f and the gravity effects on the structure parts R_g. The R_f and R_g tend to increase as the deployable structures are enlarged. The deployment force margin T is defined as the difference between F and the total deployment resistance force ($R_m + R_f + R_g$). The structure deploys under a positive value of T. However, the mass of the springs and structures increases with increases in F. Deployment force F is assumed to be $3R_m$ because the values of R_f and R_g are difficult to estimate. In this case, the structure can deploy at $R_f + R_g < 2R_m$.

Spring Torque

The installation of the helical coil springs onto the top bending bar is shown in Fig. 5. Two sets of springs are located at both sides of the top bending bar. The deploying torque, 3.14 Nm in the stowed position and 1.568 Nm when deployed, is generated by one set of coil springs. The deployment force in the deployment direction is converted from the deploying torque generated by the helical coil springs. The relationship between the deployment angle and the deployment force is shown in Fig. 6. The deployment resistance force from friction was about 5% of the deployment force. The frictional loss was obtained by comparing the torque data of the springs and the deployment force measured by the top bending bars. Calibrated push–pull gauges were used to measure the deployment force of the top bending bars. The deployment force drop caused by the gravitational force at the top bending bars was about 20% of the deployment force. The deployment force was calculated within ±5% accuracy

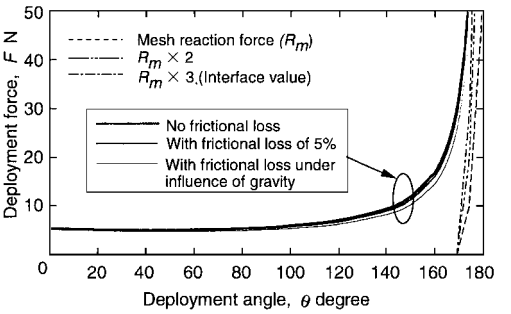

a) Deployment angle of 0–180 deg

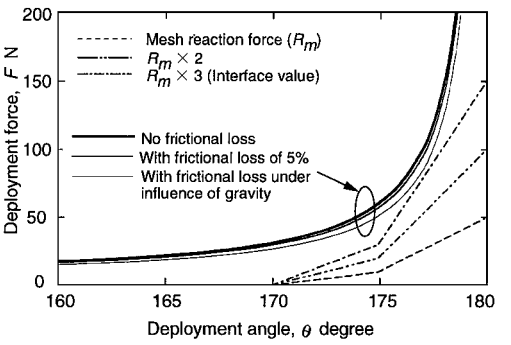

b) Deployment angle of 160–180 deg

Fig. 6 Deployment force profile of the top bending bar (calculated).

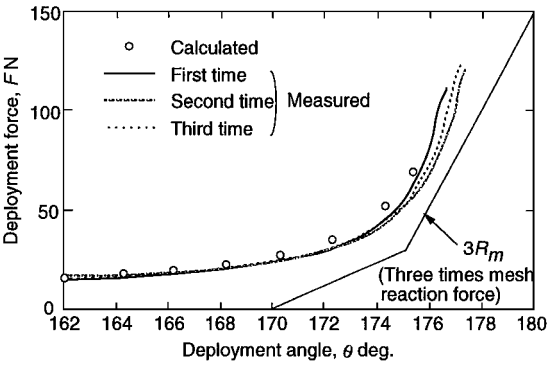

Fig. 7 Deployment force profile of the top bending bar (measured).

using the existing spring torque. Over three times the mesh reaction force as the interface value was deduced by calculations under the existing frictional loss and gravitational force at the top bending bars.

Evaluation of the Deployment Force

The deployment force design using the preceding method was evaluated by experiments using a one-sided part of the deployable structure. The deployment angle was measured by potentiometers attached to the upper hinges. The deployment force was measured by a push–pull gauge on the linear stage. The deployment angle and the deployment force are compared in Fig. 7. The deployment is complete when the deployment angles of all of the top bending bars reach 180 deg. However, the deployment angles of the top bending bars differ beyond a deployment angle of 177 deg because the latch progresses sequentially. Therefore, the measured data of the deployment force margin are plotted to a deployment angle of 177 deg. The deployment force was calculated within ±5% accuracy using the existing spring torque. The deployment force and deployment angle were measured within ±5% and ±0.1-deg accuracy using the existing hardware and instrumentation. The deployment force generated by the coil springs was confirmed as over three times that of the mesh reaction force under our measurement conditions.

Evaluation of the Mesh Reaction Force

The surface shape was adjusted to achieve the required surface accuracy of 1.0 mm rms before the deployment tests. The results of the surface adjustments are described later in this paper. The reaction forces of the surface cable and the back cable were 32.3 N and 16.7 N, and so the total value of the mesh reaction force was 49 N at the interface point of the standoff. There were some errors in the tension, the length, and the fixed position of the cable network. These errors occurred at the node fixation and tension addition when the cable networks were constructed. An error analysis was conducted to determine the permissible range of errors. The tension errors and the initial length errors of all of the cables were given at random using a regular distribution. The adjustment conditions of the surface shape were then determined, without any slack in the mesh surface under gravity conditions. The tension errors of the surface cable and the back cable were ±25 and ±35% and the length error of the cable was ±0.2 mm.

Deployment Test

Test Configuration

A magnetically suspended slider test facility[11] was used for the deployment tests of the test object. The facility was 7.5 × 8.0 m, and the height from the floor was 6 m. The test object was suspended by 24 magnetically suspended sliders. The deployment test facility enables maximum drag with a horizontal motion of less than 0.25 N and a cable tension control precision of within 0.25 N.

The deployable structure and mesh surface were constructed separately and connected to each other on the standoffs, satisfying the interface conditions described. Figure 8 shows the test configuration of the deployment test. The suspension points of the test object were determined by applying the results of previous research.[11] Twenty-four points, 12 for the outer bars and 12 for the inside pantograph bars, were suspended vertically, and the gravitational force was compensated by the magnetically suspended sliders. The gravitational force acting on the mesh surface behaves as a deployment resistance force, even if sliders are used to suspend the deployable structure. This effect appears after the deployment angle reaches 170 deg. Therefore, the mesh surface was hung by 13 points from the ceiling plate after the deployment angle reached 150 deg to reduce the deployment resistance force (13.7 N at a deployment angle of 170 deg).

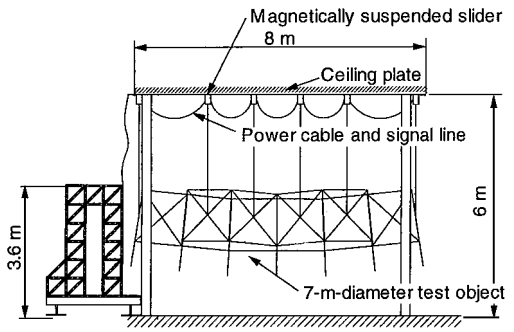

Fig. 8 Deployment test configuration.

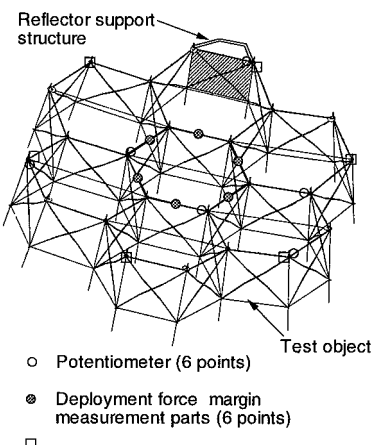

Fig. 9 Allocation of the measurement sensors.

Measurement Method

The deployment force margins (the difference between the deployment force and the deployment resistance forces) were measured in the deployment test using the 7-m test object. Strain gauges were used to measure the deployment force margin, based on the tension of the deploying velocity control cable. The deployment angle was measured by a potentiometer attached to the hinges of the top bending bars. Synchronous deployment was observed by microswitches equipped in the latch mechanisms of the top bending bars. The locations of these sensors are shown in Fig. 9.

Deployment Analysis

The deployable structure deploys under a slow movement of hinges using deploying velocity control mechanisms. The effects on the deployment force from the velocity and the acceleration of the structure are negligibly small. A quasi-static analysis, which always treats the velocity and the acceleration of the structure as zero, can be applied to provide highly accurate calculations. We used ADAMS (Mechanical Dynamics, Inc., trademark) Mechanism Analysis Software for the quasi-static deploying analysis.

Deployment Test Results

Test Results

The suspension cables cannot be positioned vertically when the test object is completely stowed because of the stowed dimensions of the 24 sliders. The deployable structure of the test object does not have any singular hinge allocations for a large deployment force or large deploying resistance force. The mesh reaction force is very small until the deployment angle reaches 150 deg. Therefore, the deployment test began at $\theta = 50$ deg and the deployment force design was mainly evaluated after $\theta = 168$ deg. Deployment takes about 20 min. The relationship between the deployment angle and the deployment force margin (the tension of the deploying velocity control cable), measured in the deployment test, is shown in Fig. 10. The deployment force and deployment angle were measured within ±5% and ±0.1-deg accuracy using existing hardware and instrumentation. The deployment force margin is always maintained within a positive value during deployment even if the value drops to less than 10 N.

As stated, the deployment resistance forces can be classified into the mesh reaction force and other resistance forces. A three-times mesh reaction force is provided to the interface value between the mesh surface and the deployable structure. The other resistance forces are classified into the frictional forces at the hinges and gravitational force acting on the mesh surface. The deployment resistance force caused by the gravitational force of the mesh surface increases as deployment progresses. The differences between the first latch and the final latch in the six latch signals in three deployment tests were 162, 172, and 156 s, although the test object was designed as

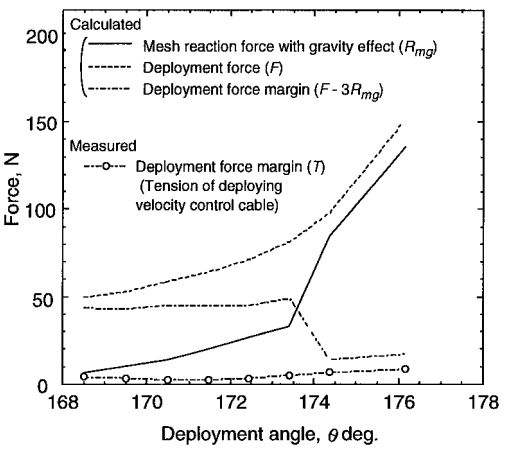

Fig. 10 Comparison of calculated and measured deployment force margins.

a synchronous deployable structure. The gravitational force compensation error of the mesh surface and the deployment resistance forces caused by asynchronization are discussed in the following section.

Gravitational Force Compensation Error of the Mesh Surface

The gravitational force acting on the mesh surface was compensated by hanging from 13 points on the mesh surface at deployment completion because of the test configuration restrictions. Therefore, the gravitational force could not be compensated perfectly at a deployment angle of 150–180 deg. The deployment resistance force was calculated after the gravitational force compensation of the mesh surface under the assumption that some mesh mass cannot be compensated near the standoffs. The suspension positions of the mesh surface for gravity compensation were placed on the positions of deployment completion. Therefore, gravity could not be compensated perfectly during deployment. The compensation error of the gravitational force was estimated at about 30% of the mesh reaction force at a deployment angle of 168 deg and decreased to 5% as deployment progressed. In a space environment, this value is added to the deployment force margin because the resistance force is not generated in microgravity conditions.

Asynchronous Effect

Asynchronicity is caused by distortion of the longitudinal bars. Twelve longitudinal bars are placed on both the outer positions and inner positions of the test object. We observed the bending of the inner longitudinal bars during the deployment test. The 12 outer bars reinforce the outer longitudinal bars of the test object. However, the inner longitudinal bars could not be reinforced because of structural restrictions. We believe that the bending of inner longitudinal bars restricts the synchronicity of the structure.

Other reasons for the bending of the inner longitudinal bars are the releasing velocity error of the control cables from the six deploying velocity control mechanisms and the imbalance in the tension of the hanging cables. The former seems to be caused by an error in the diameter of the drum in the deploying velocity control mechanism. This error is estimated at 2–4 mm because of the steps of the wound control cables in the six deploying velocity control mechanisms. Hanging the cables at 24 separate points causes this. It is difficult to eliminate these minor errors. Asynchronicity occurs for the various reasons mentioned, and the deployment resistance force increases. This value also exists in a space environment because the asynchronicity relates to the structural design. It was confirmed that a threefold mesh reaction force is necessary for the deployment force.

Achieved Characteristics of the Mesh Reflector

The test object we used was also evaluated by a surface measurement test and static load test. These tests were conducted continuously using the same test facility. The total test period was about one month, including the reappearance tests.

Mesh Surface Accuracy

The surface shape was adjusted by changing the length of the tie cords, as shown in Fig. 3. The calculations of the adjustment values and the adjustments were repeated in the shape measurements process, aiming at a surface accuracy target value of 1.0 mm rms and a deployment reappearance error of 1.0 mm rms. These values were distributed considering 1.8 mm rms of thermal distortion error, 0.3 mm rms of both measurement and moisture absorption errors, and 0.5 mm rms of gravity distortion compensation error. The surface shape was determined by measuring the 205 points on the mesh surface node, and the 12 points on the standoffs on the outside of the deployable structure using a three-dimensional optical theodolite system. The difference between the measured surface shape and the ideal surface shape was calculated to determine the adjustment values at the nodes.

The results of the surface adjustments and shape measurements are shown in Fig. 11. The measurement error allowance was within ±0.1 mm rms of the optical theodolite system. The surface shape error for the surface cable node of 205 points was reduced from 7.04 to 0.96 mm rms by making three surface adjustments. This result indicates the efficiency of the surface adjustments. The surface accuracy was also measured by repeatedly folding and unfolding the mesh surface after the surface adjustment. The surface accuracy of 0.5 mm rms was restored after three adjustments. We confirmed that the surface shape approximation error was maintained to within 1.0 mm rms, based on the deploying measurements.

Table 1 Natural frequency and vibration mode

Order	Frequency, Hz	Mode
1	0.38	Reflector, in-plane, bending (z axis)
2	0.52	Reflector, out-of-plane, bending (y axis)
3 ~ 9	1.11 ~ 1.12	Truss structure, local mode
10	1.26	Reflector, torsion (x axis)

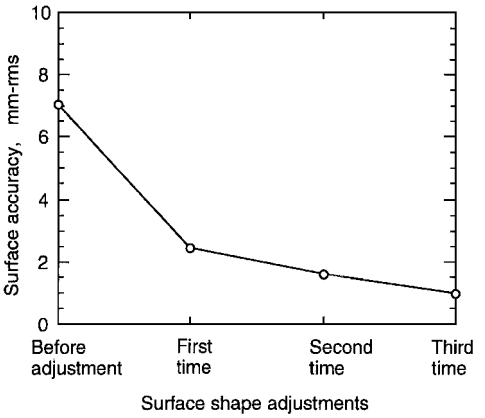

Fig. 11 Measured results of the surface shape error.

Structural Rigidity

The structural rigidity was measured by a static load test using magnetically suspended sliders. The test object was attached to the simulated satellite bus by connecting a reflector support structure. The natural frequency was calculated by MSC/NASTRAN (MacNeal–Schwendler Corp. trademark) structural analysis software using a deployed analytical model after completing the stiffness tuning. The rotation stiffness of the hinges of the reflector support structure is dominant in the in-plane distortion of the reflector. Therefore, stiffness tuning is initially conducted around the reflector support structure. Next, the rigidity of the reflector with the reflector support structure is tuned using the mesh stiffness and truss stiffness obtained from the static load test. The reflector shape was measured using a three-dimensional optical theodolite system by changing the suspension force of the test object. The suspension force was changed to +0.98, +1.96, and +0.98 N for the nominal values of the suspension force in the surface accuracy test. The measurement points of the surface shape were the 12 points of the standoffs, the 12 points of the surface nodes connected to the tie cords on the deployable structures, and the 7 points of surface nodes placed at the center of each hexagonal structure.

The parameters of the structural rigidity were the Young's modulus of each structure part, the rotation stiffness of the hinges at the reflector support structure, and the axial stiffness of the cables. These parameters are measured independently. Other parameters also contributed to the natural frequency of the test object with the reflector support structure. However, it is difficult to identify the effects of all of the parameters. Therefore, the analytical model was tuned using the preceding three parameters. The results are given in Table 1. The first natural frequency was 0.38 ± 0.1 Hz. The structure maintained sufficient structural rigidity.

The structural rigidity of a 10-m full-scale reflector was also estimated. The reflector was simulated as a disk because the reflector support structure influences reflector distortion. The equation $2\pi f_1 = (k/I)^{1/2}$ represents the relationships of k, f_1, and I. For the 7-m-diam test object, k was calculated at 6.33×10^3 Nm/rad because I was 1.11×10^3 kgm^2. For a 10-m full-scale reflector, f_1 is

Table 2 Masses of the 7-m-diam test object and a 10-m-diam full-scale reflector

Construction	7-m test object (measured), kg	10-m full-scale reflector (estimated), kg
Mesh surface	3.9[a]	11.4[b]
Twine prevention membrane	1.0	7.2
Deployable structure	30.9	47.5
Deploying velocity control mechanism	5.0	10.9
Reflector support structure	3.6	3.6
Total mass	44.4	80.6

[a]Substitute mesh. [b]Metal mesh.

0.13 ± 0.03 Hz because I was 9.18×10^3 kgm^2. We then confirmed that the first natural frequency was maintained at over 0.1 Hz, which is required for attitude control in antenna pointing.

Mass of the Mesh Reflector

Most parts of the deployable structure are comprised of carbon fiber reinforced plastics. The hinges and connecting parts are made of an aluminum alloy. The top bending bars are forced by compression, and the bottom bending bars are forced by tension applied to the lightweight design. The measured mass of the test object and the estimated mass of the full-scale reflector are shown in Table 2. The 7-m-diam test object designed and evaluated in this paper had a 44.4-kg mass. The test object was constructed using different materials than used in the flight model. The estimated mass of a 10-m full-scale reflector with the materials used for the flight model is 80.6 kg. The reflector mass achieved was less than 100 kg, which is required for the mass distribution of a 2-ton class geostationary satellite. The area of the mesh surface was 97 m^2, indicating that a 10-m class mesh reflector with a surface density of 0.79 kg/m^2 can be realized from this study.

Conclusion

This paper described the deployment characteristics of a 7-m-diam test object that is a partial model of a 10-m-diam mesh reflector with a surface accuracy of 1.0 mm rms. The surface accuracy and rigidity were also evaluated by surface measurement tests and static load tests. The test object was constructed by removing the peripheral elements from a full-scale reflector. The deploying velocity control mechanisms were placed in the same positions as they are on a full-scale reflector. Practical knowledge regarding the characteristics of a full-scale reflector was obtained from this study and is summarized as follows.

1) Three complete deployments of the 7-m test object were achieved, and control of the deploying velocity and deployment functions was demonstrated. It was confirmed that a 10-m-diam full-scale reflector with the same structural design would deploy in space.

2) The mesh reaction force was obtained as the design value. It was confirmed that the deploying resistance force caused by the gravitational force on the mesh surface was 5–30% of the mesh reaction force in the ground tests.

3) Most deployment resistance forces were caused by deploying asynchronicity. The cause of the asynchronicity was considered to be the bending of the longitudinal bars and a winding error of the cable at the drums of the deploying velocity control mechanisms. It was clarified that a deployment force at least three times the mesh reaction force is necessary for the deployment force design.

4) Surface accuracy was achieved after three courses of adjustments and measurements. Restoration of the surface accuracy after three folding and unfolding measurements was also confirmed by the test. It was determined that the full-scale reflector would achieve sufficient surface accuracy using the evaluated design method.

5) The predicted natural frequency of a 10-m full-scale reflector was achieved at 0.13 Hz, which meets the required value of over 0.1 Hz, using the test objects with a static load test and analysis.

6) The estimated mass of a 10-m-diam mesh reflector with a surface accuracy of 1.0 mm-rms error is 80.6 kg, and the achieved surface density is 0.79 kg/m^2.

Acknowledgments

The authors thank Kazuhiko Yoneyama for his encouragement and Yuichi Otsu for his advice. The authors are deeply indebted to the collaborators from Mitsubishi Electric Corporation Kamakura Works for their support and input. This work was presented as Paper IAF-97-I.1.06 at the 48th International Astronautical Congress, Turin, Italy, 7 October 1997.

References

[1]Yoneyama, K., Otsu, Y., Miyoshi, T., Kawakami, Y., Hara, H., and Hoshino, H., "R&D on S-Band Mobile Communications and Sound Broadcasting System by Geostationary Satellite for the Next Decade," 47th International Astronautical Congress, International Astronautical Federation, IAF Paper 96-M.3.04, Beijing, Oct. 1996.

[2]Kaya, N., and Maryniak, G. E., "Proposal of International Design and Arguments on Space Power (IDEAS)," 47th International Astronautical Congress, International Astronautical Federation, IAF Paper 96-R.2.02, Beijing, Oct. 1996.

[3]Hirosawa, H., and Hirabayashi, H., "VLBI Space Observatory Programme (VSOP) Satellite," *IEEE Aerospace and Electronic Systems Magazine*, Vol. 10, No. 6, 1995, pp. 17–23.

[4]Freeland, R. E., Bilyeu, G. D., and Veal, G. R., "Development of Flight Hardware for a Large, Inflatable-Deployable Antenna Experiment," *Acta Astronautica*, Vol. 38, Nos. 4–8, 1996, pp. 251–260.

[5]Higuchi, K., Natori, M. C., Hatta, H., and Yokota, R., "Inflatable Space Rigidized Structure: Adaptivity and Fundamental Experiment," *Proceedings of the 20th International Symposium on Space Technology and Science*, 20th ISTS Publications Committee, Tokyo, 1996, pp. 234–239.

[6]Onoda, J., Fu, D., and Minesugi, K., "Two-Dimensional Deployable Hexapod Truss," *Journal of Spacecraft and Rockets*, Vol. 33, No. 3, 1996, pp. 416–421.

[7]Natori, M. C., Takano, T., Inoue, T., and Kitamura, T., "Deployable Mesh Antenna Structure for MUSES-B Spacecraft," 46th International Astronautical Congress, International Astronautical Federation, IAF Paper 95-I.1.04, Oslo, Norway, Oct. 1995.

[8]Akaishi, A., Okamoto, T., Tanizawa, K., Ebisui, T., and Ohkubo, K., "Scale Model Characteristics of Large Deployable Mash Reflector Antenna," *Proceedings of the 19th International Symposium on Space Technology and Science*, 19th ISTS Publications Committee, Tokyo, 1994, pp. 711–716.

[9]Watanabe, M., Meguro, A., Mitugi, J., and Tsunoda, H., "Module Composition and Deployment Method on Deployable Modular-Mesh Antenna Structures," *Acta Astronautica*, Vol. 39, No. 7, 1996, pp. 497–505.

[10]Tsunoda, H., Meguro, A., Miyasaka, A., and Watanabe, M., "Large Deployable Antenna Configuration for Future Communication Satellite," 47th International Astronautical Congress, International Astronautical Federation, IAF Paper 96-I.1.02, Beijing, Oct. 1996.

[11]Tsunoda, H., Hariu, K., Kawakami, Y., Miyoshi, K., Nakagawa, J., and Sugimoto, T., "Deployment Test Methods for a Large Deployable Mesh Reflector," *Journal of Spacecraft and Rockets*, Vol. 34, No. 6, 1997, pp. 811–816.

[12]Ebisui, T., Iso, A., Orikasa, T., and Okamoto, T., "Characteristics of Deployable Mesh Reflector Antenna Models for Future Mobile Communications Satellite," *Transactions of the Japan Society for Aeronautical and Space Sciences*, Vol. 39, No. 123, 1996, pp. 101–112.

R. B. Malla
Associate Editor